Inorganic Chemistry, Vol. 17, No. 6, 1978 **1613**

Contribution from Bell Laboratories,
Holmdel, New Jersey 07733

The Iodine Coordination Polyhedron in Hydrated Sodium Periodate Determined from Second Harmonic Generation

G. R. CRANE* and J. G. BERGMAN

Received June 20, 1977

Applications of optical second harmonic generation (SHG) to the study of solid-state sterochemical problems have been recently reported. This paper will describe the use of SHG to distinguish between different types of possible coordination polyhedra. In particular, we will show that the iodine coordination in hydrated sodium periodate is not tetrahedral ($NaIO_4 \cdot 3H_2O$) but is octahedral $NaH_3O[IO_3(OH)_3]$ as recently suggested by Poulet and Mathieu from Raman measurements.

Introduction

The use of optical second harmonic generation (SHG) to study solid-state sterochemical problems such as tetrahedral rotations[1,2] and distortions of both tetrahedra[3] and octahedra[4] in crystals has been recently reported. This paper will demonstrate that SHG can also be used to distinguish between different types of possible coordination polyhedra. In particular, we will show that the iodine coordination in hydrated sodium periodate is not tetrahedral ($NaIO_4 \cdot 3H_2O$) but is octahedral $NaH_3O[IO_3(OH)_3]$ as recently suggested by Poulet and Mathieu[5] from Raman measurements.

SHG is the process whereby light at some frequency 2ω is produced as the response of some nonlinear, acentric, medium to a driving field at frequency ω. SHG is usually characterized by a macroscopic polarizability d_{ijk} (nonlinear coefficient) which is a third rank tensor relating second harmonic polarization to terms quadratic in fundamental electric field. The nonlinear coefficient tensor is always symmetric for interchange of the last two indices[6] and is usually[7] (within experimental uncertainty) fully symmetric (Kleinman[8] symmetry). Additional symmetries arise due to symmetry of the nonlinear medium.

The bond polarizability model is well established[9] for linear optical polarizabilities of molecules. This model describes the macroscopic linear polarizability as a (tensor) sum of the linear polarizabilities of the individual covalent bonds in the medium

$$\chi_{ij} = V^{-1} a_{il} a_{jm} \alpha_{lm} \tag{1}$$

where χ and α are macroscopic and microscopic (bond) polarizabilities, respectively, V is volume, and (a_{ij}) is a transformation matrix. The extension[10-12] of this model to second-order polarizability begins by recognizing that this effect must originate in the valence electrons of the system since their environments are so much more acentric than those of the core electrons. Hence, the analogous relation to eq 1 is

$$d_{ijk} = V^{-1} a_{il} a_{jm} a_{kn} \beta_{lmn} \tag{2}$$

where d and β are respectively macroscopic and microscopic bond polarizabilities.[20] The structural dependence of the transformation matrix (a_{ij}) combined with measurements of nonlinear coefficients (d_{ijk}), allows one to obtain structural information.

Theory

The interaction between light and dielectric media is generally described in terms of the induced dipole moment P which is expressed as a power series in field E by

$$P = P_0 + \chi E + dE^2 + \Gamma E^3 + \ldots \tag{3}$$

where P_0 is a spontaneous dipole moment, χ is the linear polarizability, and d, Γ ... are hyperpolarizabilities.[10] This paper will concern itself with the quadratic term d which is responsible for two frequency mixing or, in a limiting case, second harmonic generation (SHG).

If we consider a field with harmonic time dependence $E = E_0 \cos(\omega t)$ then

$$E^2 = {}^1/_2 E_0^2 [1 + \cos(2\omega t)] \tag{4}$$

Substituting this into eq 3, we see that the first term generates the phenomenon of optical rectification, while the second term gives rise to second harmonic generation (SHG). We then define a macroscopic nonlinear polarizability d_{ijk} by the relation

$$P_i(2\omega) = \sum_{jk} d_{ijk} E_j(\omega) E_k(\omega) \tag{5}$$

where i, j, and k refer to coordinate axes. Due to the symmetry in eq 5 between indices j and k, there can be at most 18 independent components.[6] Under these conditions it is customary[13] to contract d_{ijk} to a 3×6 matrix (d_{ij}) by the method shown schematically by

$$\begin{bmatrix} d_{i11} & d_{i12} & d_{i13} \\ \cdot & d_{i22} & d_{i23} \\ \cdot & \cdot & d_{i33} \end{bmatrix} \rightarrow \begin{bmatrix} d_{i1} & d_{i6} & d_{i5} \\ \cdot & d_{i2} & d_{i4} \\ \cdot & \cdot & d_{i3} \end{bmatrix}$$

The second harmonic polarization is then given by

$$P_i(2) = d_{i1} E_x^2 + d_{i2} E_y^2 + d_{i3} E_z^2 + 2d_{i4} E_y E_z + 2d_{i5} E_x E_z + 2d_{i6} E_x E_y \tag{6}$$

The microscopic polarizability corresponding to d_{ijk} is β_{ijk} (again symmetric in j and k indices). The bond additivity model in this case assumes each bond to be represented by a polarizability of the (contracted) form

$$\beta_{ij} = \begin{bmatrix} 0 & 0 & 0 & 0 & \beta_{31} & 0 \\ 0 & 0 & 0 & \beta_{31} & 0 & 0 \\ \beta_{31} & \beta_{31} & \beta_{33} & 0 & 0 & 0 \end{bmatrix} \tag{7}$$

where bond symmetry C_∞ and Kleinman symmetry have been assumed.

The macroscopic (crystal or molecule) polarizability is then given as the (tensor) sum of the individual bond polarizabilities. Specifically

$$d_{ijk} = V^{-1} \sum_s \left[\sum_{p,q,r} a_{ip} a_{jp} a_{kr} \beta_{pqr} \right] \tag{8}$$

where the sum is over bonds, s. V is the unit cell volume and (a_{ij}) is the matrix of the transformation from the bond coordinate system[21] to the crystal coordinate system.

A closed form expansion of eq 8 is

$$d_{ijk} = V^{-1} \sum_s \{ \gamma_i \gamma_j \gamma_k (\beta_{33} - 3\beta_{31}) + (\gamma_i \delta_{jk} + \gamma_j \delta_{ki} + \gamma_k \delta_{ij}) \beta_{31} \} \tag{9}$$

where γ_i is the ith direction cosine of bond s, δ_{ij} is the Kro-

0020-1669/78/1317-1613$01.00/0

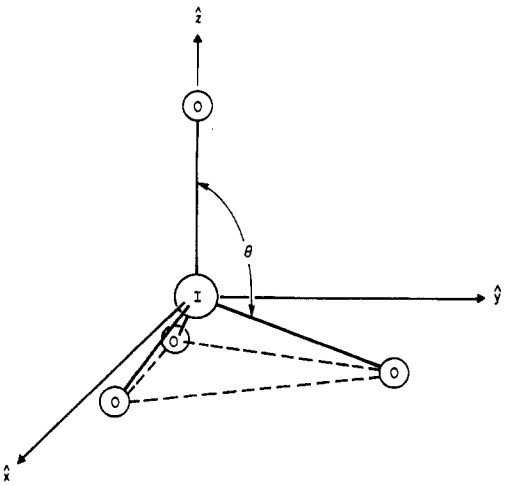

Figure 1. The tetrahedral $[IO_4]$ ion.

necker delta, $\delta_{ij} = 1$ if $i = j$, $= 0$ otherwise. The direction cosines of eq 9 are the structurally sensitive part of the bond additivity model.

Hydrated sodium periodate crystallizes in space group $R3\text{-}C_3^4$ with one formula unit per rhombohedral cell.[14] The nonlinear coefficients (assuming Kleinman symmetry) are given by the array[13]

$$d_{ij} = \begin{bmatrix} d_{11} & d_{12} & 0 & 0 & d_{15} & d_{16} \\ d_{21} & d_{22} & 0 & d_{24} & 0 & d_{25} \\ d_{31} & d_{32} & d_{33} & 0 & 0 & 0 \end{bmatrix} \tag{10}$$

where $-d_{11} = d_{12} = 2d_{26}$, $-d_{22} = d_{21} = 2d_{16}$ and $d_{31} = d_{32} = d_{24} = d_{15}$. There are four independent nonlinear coefficients here. Using eq 9 these are found to be given by the relations

$$d_{11} = V^{-1} \sum_{\text{bonds}} \{l^3(\beta_{33} - 3\beta_{31}) + 3l\beta_{31})\} \tag{11}$$

$$d_{22} = V^{-1} \sum_{\text{bonds}} \{m^3(\beta_{33} - 3\beta_{31}) + 3m\beta_{31}\} \tag{12}$$

$$d_{33} = V^{-1} \sum_{\text{bonds}} \{n^3(\beta_{33} - 3\beta_{31}) + 3n\beta_{31}\} \tag{13}$$

$$d_{31} = V^{-1} \sum_{\text{bonds}} \{nl^2(\beta_{33} - 3\beta_{31}) + n\beta_{31}\} \tag{14}$$

where $\{l, m, n\}$ are the direction cosines of the individual bonds with respect to the x, y, and z axes, respectively. Since nonlinear polarizability is correlated to linear polarizability and since the linear polarizability is primarily due to the iodine in this system, we can restrict the summation in eq 11–14 to the I–O bonds. It is the sensitivity of these four equations to the iodine–oxygen coordination which can be exploited to determine whether the iodine is tetrahedrally coordinated as originally assumed[14] (prior to the present work, the structure had not been determined) or octahedrally coordinated as asserted by Poulet and Matheiu.[5]

Assume first that the iodine atom is tetrahedrally coordinated. In this case, one I–O bond must lie on the crystallographic $\hat{z}$ axis[14] as depicted in Figure 1. Then the bond additivity relations 11–14 are readily evaluated in terms of the principal O–I–O angle θ, or since we expect this angle to be near 109.5° (the tetrahedral angle) it is convenient to evaluate these relations as functions of $\delta\theta = \theta - 109.5°$. The details of this are given in the Appendix. One point to notice here is that for $\delta\theta = 0$, that is an undistorted tetrahedron, the nonlinear coefficients d_{33}, d_{22}, and d_{31} are in the ratios of 2:1.41:−1, respectively. This relation is independent of any assumption of particular bond polarizabilities.

In order to compare this model with experiment, we need to know the I–O bond polarizabilities. For this, we assume

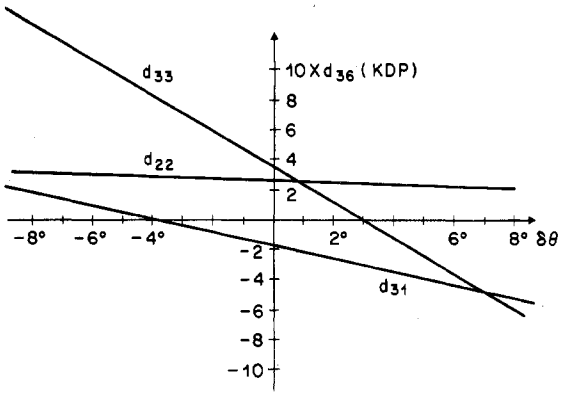

Figure 2. Calculated nonlinear coefficients for tetrahedral coordination in $Na(IO_4)\cdot 3H_2O$ as a function of the trigonal distortion $\delta\theta$.

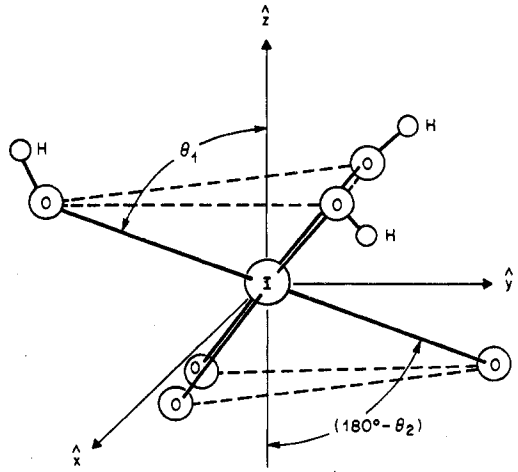

Figure 3. The octahedrally coordinated $[IO_3(OH)_3]^{2-}$ ion.

that, in the I(+5) compounds, the oxygens have already polarized the iodine valence electrons to very near their saturation point so that changing to a formal charge of +7 should not drastically alter the I–O bond hyperpolarizability. Hence, we assume I–O polarizabilities[12] of $\beta_{33} = 34.5 \times 10^{-28} m^3 d_{36}(\text{KDP})$ and $\beta_{31} = 9.65 \times 10^{-28} m^3 d_{36}(\text{KDP})$. (This assumption will be seen to be justified by the subsequent close agreement between the calculated and the experimentally measured nonlinear coefficients.) The coefficients calculated from eq 11–14 and the above bond polarizabilities are shown for the tetrahedral model in Figure 2.

If we assume, on the other hand, that the iodine is octahedrally coordinated, then we consider the system shown in Figure 3. We expect that θ_1 and θ_2 are near 54.74 and 125.26°, respectively, i.e., $\delta\theta \sim 5°$. Hence it is convenient to solve eq 11–14 in terms of $\delta_1 = \theta_1 - 54.74°$ and $\delta_2 = \theta_2 - 125.26°$. One particular feature of this solution is that the ratios of the nonlinear coefficients are strictly fixed by the ratios of the bond polarizabilities and are independent of δ_1 and δ_2. The details of this are also given in the Appendix.

Again assuming I–O polarizabilities as in the tetrahedral model we find solutions to 11–14 shown graphically in Figure 4 as a function of the "average" distortion given by $\delta\theta = (\delta_1 + \delta_2)/2$. Comparison of Figure 2 with Figure 4 indicates that measurement of the nonlinear coefficients of this material ought to immediately reveal which is the correct iodine coordination. This is even more apparent from Figures 5 and 6 which show the ratios of the nonlinear coefficients calculated from the two models.

One experimental difficulty, however, must be dealt with. The coordinate systems used to solve eq 11–14 were chosen for convenience so as to have one of the I→O bonds in the (y, z) plane.

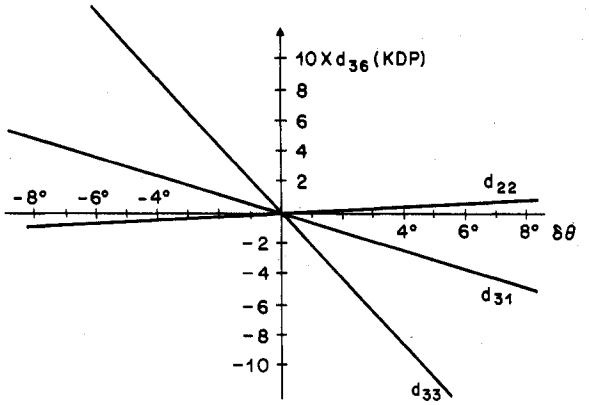

Figure 4. Calculated nonlinear coefficients for octahedral coordination as a function of the average trigonal distortion angle $\delta\theta$.

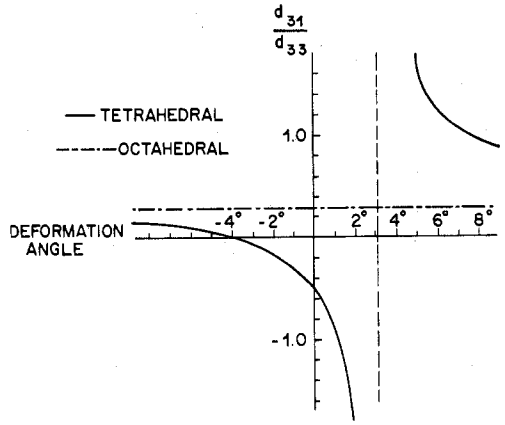

Figure 5. The calculated ratio d_{31}/d_{33} compared for the tetrahedral and octahedral models.

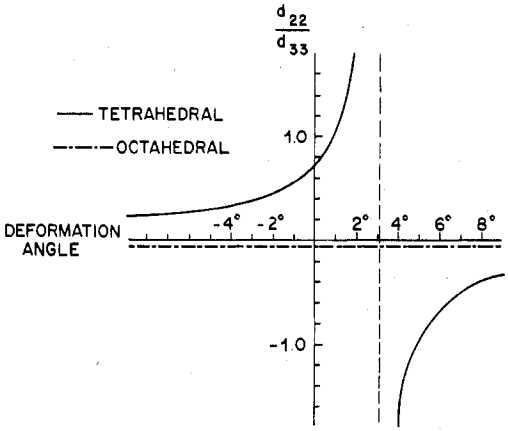

Figure 6. The calculated ratio d_{22}/d_{33} compared for the tetrahedral and octahedral models.

Since we do not know the relation of this "molecular" coordinate system (mol) to the crystallographic coordinate system or the laboratory coordinate system (lab) we must reevaluate eq 11 and 12 in the laboratory system. Assuming that this system is related to the "molecular" system by a rotation of ϕ (about the $\hat{3}$ axis) it is readily shown that

$$d_{11}(\text{lab}) = d_{22}(\text{mol}) \sin(3\phi) \tag{15}$$

and

$$d_{22}(\text{lab}) = d_{22}(\text{mol}) \cos(3\phi) \tag{16}$$

Hence it is the quantity

$$\{d_{11}^2(\text{lab}) + d_{22}^2(\text{lab})\}^{1/2} = d_{22}(\text{mol}) \tag{17}$$

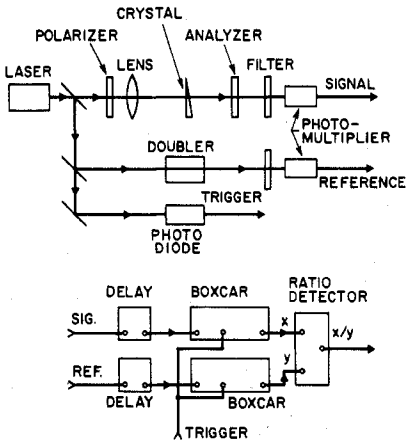

Figure 7. Schematic of the experimental apparatus.

which is to be compared with the curves of Figures 2 and 4.

Experimental Section

Two ~2.5° wedges of the crystal were prepared, one with face normal to the $\hat{x}$ axis and the other with its face normal to the $\hat{y}$ axis. A general requirement for sample preparation is that the surfaces be flat to within a small fraction of the smallest coherence length to be measured and smooth enough to allow reasonable beam transmission. The first wedge allowed measurement of coefficients d_{22}, d_{32} ($=d_{31}$), and d_{33} while the second allowed measurement of d_{11}, d_{31}, and d_{33}. To measure a nonlinear coefficient, the wedge was placed in one branch of the dual beam optical system of Figure 7. The second harmonic light from the crystal and the reference crystal (phase matched $LiIO_3$) were detected by photomultipliers and twin boxcar integrators, and the ratio of the outputs was recorded as the wedge was translated across the beam. The resulting set of maxima and minima are a measure of the nonlinear coefficient and coherence length l_{ij}, the latter being related to the translation distance Δt between maxima (or minima) and the wedge angle θ by

$$|l_c| = {}^1/_2 \Delta t \tan\theta \tag{18}$$

Relative nonlinear coefficients were then found from the peak second harmonic intensities by the equation[15]

$$\frac{d_{ij}^{\text{A}}}{d_{ij}^{\text{B}}} = \left[\frac{I_{ij}^{\text{A}}}{I_{ij}^{\text{B}}}\right]^{1/2}\left[\frac{l_{ij}^{\text{B}}}{l_{ij}^{\text{A}}}\right]\left[\frac{n_{\text{A}}(\omega)+1}{n_{\text{B}}(\omega)+1}\right]^2\left[\frac{n_{\text{A}}(2\omega)+1}{n_{\text{B}}(2\omega)+1}\right] \tag{19}$$

where $n_A(\omega)$ is the index of refraction of crystal A at frequency ω. The sign of coefficient d_{31} was determined by interference methods[16] to be the same as d_{33}. In order to determine the magnitude of the nonlinear coefficients, the second harmonic intensities were compared (via eq 19) to the second harmonic from a quartz wedge standard. The experimental results are given in Table I where we have used $d_{11}(\alpha\text{-}SiO_2) = 0.8 d_{36}(KDP)$.[17] The uncertainties were determined from the signal to noise ratio of the experiments.

The indices of refraction to be used in eq 19 were estimated by measuring the visible birefringence with a Zeiss polarizing microscope and Ehringhaus compensator which yielded $n^e - n^o = 0.036$ ($n^o = n_x = n_y$; $n^e = n_z$). The mean index $\langle n\rangle = {}^1/_3(n^e + 2n^o)$ was estimated via the Dale–Gladstone formula[18] to be 1.652. Combining these results gives $n^e(0.53\ \mu) \simeq 1.676$ and $n^o(0.53\ \mu) \simeq 1.640$. These indices were then combined with the measured coherence lengths l_{33} and l_{31} to give indices of refraction at 1.064 μ via

$$l_{ij} = \frac{\lambda}{4[n_i(2\omega) - n_j(\omega)]} \tag{20}$$

These indices were $n^e(1.06\ \mu) = 1.644$ and $n^o(1.06\ \mu) = 1.614$. These indices were then used to calculate the reflection corrections of eq 19 and to calculate the unobserved coherence lengths l_{11} and l_{22} given in Table I. The upper limits for d_{11} and d_{22} were then obtained by assuming that the corresponding second harmonic intensities I_{11} and

Table I. Nonlinear Coefficients, d_{ij},[a] and Coherence Lengths, l_{ij}, for $NaH_3O[IO_3(OH)_3]$

l_{11}	10.2 μ[b]	d_{11}	<0.1
l_{22}	10.2 μ[b]	d_{22}	<0.1
l_{33}	8.1 8μ	d_{33}	4.5
l_{31}	4.3 0μ	d_{31}	1.4

[a] d_{ij} in units of d_{36}(KDP) ±30% (d_{33}/d_{31} accurate to 10%). [b] Calculated from indices of refraction.

I_{22} were less than or equal to the noise measured under the appropriate experimental conditions.

Conclusions

Examination of the nonlinear coefficients of Table I shows two particularly significant points: first, $d_{33} \simeq +3d_{31}$, second, d_{22} (and d_{11}) are very small (i.e., $\leq 0.02d_{33}$). By comparison with the predictions of Figures 2, 4, 5, and 6, it is apparent that the iodine must be octahedrally rather than tetrahedrally coordinated. Furthermore, from the magnitudes of these coefficients, we see from Figure 4 that this does not require a large distortion of the octahedron, i.e., $\delta\theta \simeq 2°$. It is also interesting to note the internal consistency of the octahedral model and the experimental results. Specifically, in the model assumed we do not actually know the bond polarizabilities β_{33} and β_{31}. Nonetheless, in this model, solving eq 12 through 14 gives us d_{22} as a function of d_{33} and d_{31}.

This expression is

$$d_{22} = \frac{2^{1/2}}{4}(d_{33} - 3d_{31}) \tag{21}$$

The experimental observation that $d_{22} \simeq 0$ then implies that $d_{33} \simeq 3d_{31}$ which agrees (within experimental uncertainty) with the observed ratio $d_{33} = 3.3d_{31}$. Upon completion of this work, the crystal structure determination was undertaken by Bernstein, Abraham, and Lissalde. Their results confirm the octahedral coordination in this system.[19]

In summary, we have demonstrated that nonlinear optics or, in particular, second harmonic generation can be used as a simple, definitive tool for structural chemistry. Specifically, we have shown here that SHG can be used to determine coordination polyhedra. Additionally, when used in conjunction with conventional techniques, such as X-ray diffraction, to study the details of solid-state phase transitions the tool (SHG) may be particularly useful since once the structure is known at a particular temperature, changes with temperature can be more readily monitored optically than with X-rays; hence one can study rotations and deformations of coordination polyhedra in crystal phase transitions. Furthermore, since the bond polarizability does in fact depend only on the valence or bonding electrons which are in asymmetric environments, a better understanding of bond polarizability will afford deeper insights into the nature of bonding forces themselves. The possibilities in transition element materials are as yet largely unexplored. However, as long as the material is reasonably transmitting (i.e., crystal thinner than the absorption length) for the fundamental and the second harmonic, it is hoped that SHG might be a useful tool here as well.

Appendix

The starting point for evaluating eq 11–14 in the text is the set of bond direction cosines. For the tetrahedron of Figure 1, the complete set is the set of vectors (0, 0, 1), (0, m_0, n_0), [$(3/4)^{1/2}m_0$, $-{}^1/_2m_0$, n_0], and [$-(3/4)^{1/2}m_0$, $-{}^1/_2m_0$, n_0] where the latter two vectors are obtained by 120° rotations of the second vector around the $\hat{z}$ axis. It then follows that

$$\Sigma l^3 = \Sigma l = \Sigma m = 0 \tag{A1}$$

It follows immediately that d_{11} (via eq 11) is identically zero. Next we recognize that

$$\Sigma m^3 = {}^3/_4 m_0{}^3 \tag{A2}$$

$$\Sigma n^3 = 3n_0{}^3 + 1 \tag{A3}$$

$$\Sigma n = 3n_0 + 1 \tag{A4}$$

$$\Sigma nl^2 = {}^3/_2 n_0 m_0{}^2 \tag{A5}$$

In fact, eq A2–A5 contain only one independent variable, namely, n_0, since $m_0{}^2 = 1 - n_0{}^2$.

We proceed further by setting $n_0 = \cos\theta$ and expanding around $\theta = 109.5°$. Then

$$n_0 = \cos(109.5° + \delta\theta) = \cos(109.5°)\cos\delta\theta - \sin(109.5°)\sin\delta\theta \tag{A6}$$

and for θ very small

$$n_0 = -{}^1/_3 + \delta n$$

where

$$\delta n \cong -\delta\theta \sin(109.5°) \tag{A7}$$

Then to first order

$$n_0{}^3 = -(1/3)^3 + 3(1/3)^2\,\delta n \tag{A8}$$

It then follows that explicit solutions to eq 12–14 are respectively

$$d_{22} = V^{-1}\left\{\frac{4(2^{1/2})}{9}(\beta_{33} - 3\beta_{31}) - \frac{2^{1/2}}{2}(\sin 109.5°)(\beta_{33} - 3\beta_{31})\delta\theta\right\} \tag{A9}$$

$$d_{33} = V^{-1}\left\{\frac{8}{9}(\beta_{33} - 3\beta_{31}) - (\sin 109.5°)(\beta_{33} + 6\beta_{31})\delta\theta\right\} \tag{A10}$$

$$d_{31} = V^{-1}\left\{-\frac{4}{9}(\beta_{33} - 3\beta_{31}) - (\sin 109.5°)\beta_{33}\delta\theta\right\} \tag{A11}$$

For the octahedral case, we consider the bonds with direction cosines of (0, m_1, n_1) and (0, m_2, n_2) where m_1, m_2 and n_1, n_2 are of opposite sign and nearly equal magnitudes. The remaining two pairs of bond vectors are found again by 120° rotations about the $\hat{z}$ axis. It is obvious that (A1) still holds and that consequently d_{11} is still zero. Equations A2–A5 are then modified to

$$\Sigma m^3 = \frac{3}{4}\left[m_1{}^3 + m_2{}^3\right] \tag{A12}$$

$$\Sigma n^3 = 3\left[n_1{}^3 + n_2{}^3\right] \tag{A13}$$

$$\Sigma n = 3\left[n_1 + n_2\right] \tag{A14}$$

$$\Sigma nl^2 = \frac{3}{2}\left[n_1 m_1{}^2 + n_2 m_2{}^2\right] \tag{A15}$$

As in the tetrahedral case, we let $n_1 = \cos\theta_1$ and $n_2 = \cos\theta_2$ and expand around $\theta_1 = 54.7°$ and $\theta_2 = 125.3°$ and make use of relations analogous to eq A7, namely,

$$n_1 = \frac{1}{3^{1/2}} + \delta n_1 \tag{A16}$$

$$n_2 = -\frac{1}{3^{1/2}} + \delta n_2 \tag{A17}$$

where $\delta n_{1,2}$ = (sin 54.7°) $\delta\theta_{1,2}$ and using the first-order expansion analogous to A8 we "solve" eq 12–14 as

$$d_{22} = \frac{3(2^{1/2})}{4}(\sin 54.7^\circ)V^{-1}(\beta_{33} - 3\beta_{31})(\delta\theta_1 + \delta\theta_2) \quad \text{(A18)}$$

$$d_{33} = -3(\sin 54.7^\circ)V^{-1}\beta_{33}(\delta\theta_1 + \delta\theta_2) \quad \text{(A19)}$$

$$d_{31} = -3(\sin 54.7^\circ)V^{-1}\beta_{31}(\delta\theta_1 + \delta\theta_2) \quad \text{(A20)}$$

Registry No. $NaIO_4 \cdot 3H_2O$, 13872-31-6; $NaH_3O[IO_3(OH)_3]$, 34410-79-2.

References and Notes

(1) J. G. Bergman and G. R. Crane, *Chem. Phys. Lett.*, **41**, 133–136 (1976).
(2) G. R. Crane and J. G. Bergman, *J. Appl. Crystallogr.*, **9**, 476 (1976).
(3) J. G. Bergman and J. S. Wood, *J. Chem. Soc., Chem. Commun.*, 457 (1976).
(4) J. G. Bergman, *J. Am. Chem. Soc.*, **98**, 1054 (1976).
(5) H. Poulet and J. P. Mathieu, *J. Raman Spectrosc.*, **2**, 81–92 (1974).
(6) J. F. Nye, "Physical Properties of Crystals", Oxford University Press, London, 1957.
(7) F. G. Parsens, E. Y. Chen, and R. K. Chang, *Phys. Rev. Lett.*, **27**, 1436 (1971).
(8) D. A. Kleinman, *Phys. Rev.*, **126**, 1977 (1962).
(9) R. J. W. LeFèvre, *Adv. Phys. Org. Chem.*, **3**, 1–90 (1965).
(10) A. D. Buckingham and B. J. Orr, *Q. Rev., Chem. Soc.*, **21**, 195, (1976).
(11) F. N. H. Robinson, *Bell Syst. Tech. J.*, **46**, 913 (1967).
(12) J. G. Bergman and G. R. Crane, *J. Chem. Phys.*, **60**, 2470–2474 (1974).
(13) J. G. Bergman, Jr., and S. K. Kurtz, *Mater. Sci. Eng.*, **5**, 235–250 (1969/70).
(14) R. Burgers, *Proc. R. Soc. London, Ser. A*, **116**, 553–586 (1927).
(15) G. D. Boyd, H. Kasper, and J. H. McFee, *IEEE J. Quantum Electron.*, **QE-7**, 563–573 (1971).
(16) G. R. Crane, *J. Appl. Phys.*, **44**, 915–196 (1973).
(17) J. Jerphagnon and S. K. Kurtz, *Phys. Rev.*, **113**, 1738–1744 (1970).
(18) E. S. Larsen and H. Berman, *U.S. Geol. Surv., Bull.*, **No. 848**, 254 (1934).
(19) J. L. Bernstein, S. C. Abrahams, and F. Lissalde, submitted for publication.
(20) We note here that this expression has absorbed local field corrections and hence β is an "effective bond polarizability".
(21) The polarizability of eq 7 is given in a coordinate system where $\hat{z}$ is the symmetry axis.

Contribution from the Department of Chemistry, University of Berne, CH-3000 Berne 9, Switzerland

Jahn–Teller Effect in the $^4T_{2g}$ State of Chromium(III) in Dicesium Sodium Indium(III) Hexachloride

HANS U. GÜDEL* and TIMOTHY R. SNELLGROVE

Received September 12, 1977

Low-temperature absorption and luminescence spectra are reported for the $^4A_{2g} \leftrightarrow {}^4T_{2g}$ transition of $CrCl_6^{3-}$ doped into the elpasolite salt $Cs_2NaInCl_6$. Four magnetic dipole origins are assigned at 11 882, 11 890, 11 904, 11 916 cm^{-1}, and the vibronic sidebands of the luminescence spectra are assigned to progressions in a_{1g} and e_g modes on t_{1u} and t_{2u} false origins with frequencies 297, 240, 187, and 120 cm^{-1}. The splitting of the $^4T_{2g}$ state is smaller than expected from calculations using the full d^3 matrix. Using the effective Hamiltonian formalism, we show that the splittings may be reproduced by introducing a Ham reduction factor for off-diagonal matrix elements of $\hat{H}_{eff}$. The Jahn–Teller interaction is compatible with the presence in the luminescence of a progression in the e_g (Jahn–Teller active) mode. The Jahn–Teller energy calculated from the observed splittings is 310 cm^{-1} and that from intensity ratios in the e_g progression 264 cm^{-1}, justifying the treatment of the spin–orbit interaction as small compared with E_{JT}.

Introduction

The elpasolite salts Cs_2NaMCl_6, containing octahedral MCl_6^{3-} complexes, are useful high-symmetry host lattices for the study of trivalent transition-metal ions. The visible and MCD spectra of Cr^{3+} doped into Cs_2NaYCl_6 and $Cs_2NaInCl_6$ have been extensively studied.[1,2] In $CrCl_6^{3-}$ the value of Dq is low and the $^4T_{2g}$ state is found to be the first excited state, 12 000 cm^{-1} above the $^4A_{2g}$ ground state. We have obtained the luminescence spectrum of this transition and the absorption spectrum of a thick crystal in the same region. The $^4T_{2g}$ state splits into E′, U′($^5/_2$), U′($^3/_2$), and E″ states under the influence of spin–orbit coupling. The MCD and absorption spectra are thus complicated superpositions of the vibronic intensity from all four transitions whereas the luminescence spectrum at low temperature contains only vibronic structure from the lowest energy electronic transition. The sensitivity of the luminescence experiment is such that we can measure the vibronic spectrum due to lattice modes in the crystal.

In spite of the observation of progressions in the e_g mode as well as the a_{1g} mode of $CrCl_6^{3-}$ in the MCD spectra, previous work has neglected the Jahn–Teller interaction in the interpretation of this transition. We find our results can only be explained by considerable quenching of the spin–orbit interaction due to the Ham effect, as observed in other T_{2g} and T_{1g} states of octahedral 3d ions.[3,4]

Experimental Section

$Cs_2NaInCl_6$:Cr was kindly prepared by Woodwark.[5] The crystal was grown by the Bridgeman technique. Analysis for chromium using atomic absorption spectroscopy showed a concentration around 5 atom %. The boule contains a considerable percentage of Cr^{2+},[6] which we observe as a strong broad band in the near-IR absorption spectrum. The Cr^{3+} concentration may well be less than 5%. Absorption spectra were measured on 2 and 5 mm thick crystals with a Cary 17 spectrophotometer, equipped with a red-sensitive photomultiplier tube (RCA C31025C). Luminescence spectra were excited with a 150-W sealed-beam Xe arc (Varian) filtered with a Spex Minimate. The luminescence was dispersed with a $^3/_4$-m single Spex monochromator, with a grating blazed at 750 nm. An EMI 9684B photomultiplier (S1 response) cooled to −70 °C was used to detect the luminescence. High-resolution spectra were recorded between 830 and 880 nm using a RCA C31034 photomultiplier cooled to −30 °C. The crystals were cooled using a helium gas flow technique.

Results

Figure 1 shows the broad-band luminescence spectrum. We assign this in terms of the weak pure electronic transitions, two strong vibronic false origins, and progressions in a_{1g} and e_g modes. Figures 2 and 3 show the detailed absorption and luminescence spectra in the region where these overlap. The four bands at 11 882, 11 890, 11 904, and 11 916 cm^{-1} are found in absorption and luminescence spectra. The oscillator strengths in absorption are 1.6, 1.6, 0.9, and 0.9 × 10^{-9} for the four origins. In the luminescence spectrum the intensities vary with temperature according to a Boltzmann distribution among levels at 0, 8, 21, and 34 cm^{-1}. The vibronic sideband at the right of Figure 3 shows a similar temperature dependence, hot bands appearing at the high-energy side of the band with equal spacing and similar relative intensity as the origins. The second intense false origin at 187 cm^{-1} gives a similar pattern. We cannot assign the hot bands in the lu-

0020-1669/78/1317-1617$01.00/0
